Eur. Phys. J. B **37**, 25–37 (2004)
DOI: 10.1140/epjb/e2004-00027-y

THE EUROPEAN PHYSICAL JOURNAL B

Single-crystal structural study of the pressure-temperature-induced dimerization of C_{60}

R. Moret[1,a], P. Launois[1], T. Wågberg[1,2,b], B. Sundqvist[2], V. Agafonov[3], V.A. Davydov[4], and A.V. Rakhmanina[4]

[1] Laboratoire de Physique des Solides, UMR CNRS 8502, bâtiment 510, Université Paris-Sud, 91405 Orsay, France
[2] Department of Physics, Umeå University, 90187 Umeå, Sweden
[3] Laboratoire de Chimie Physique, Faculté de Pharmacie de l'Université de Tours, 31 av. Monge, 37200 Tours, France
[4] Institute of High Pressure Physics, Russian Academy of Sciences, 142092 Troitsk, Moscow Region, Russian Federation

Received 3 October 2003
Published online 19 February 2004 –

Abstract. We present a study by Raman spectroscopy and X-ray diffraction/diffuse scattering of C_{60} single-crystals treated at high-pressure and high-temperature. This allowed us to obtain structural information on the C_{60} dimer state which can be considered as an intermediate state in the polymerization process. In the 1–6 GPa pressure range the crystals are primarily formed of dimers with additional minor fractions of monomers, 1D and 2D polymers, as shown by the analysis of the Raman spectra. The dimers are disordered within an average cubic lattice derived from that of the monomer. Single-crystal diffraction patterns reveal a characteristic diffuse scattering intensity distribution which has been simulated by calculating the diffuse scattering produced by dimer and trimer model structures. Satisfactory agreement is obtained for random positional and orientational disorder of the C_{60}-C_{60} dimers although a small concentration of similarly disordered trimers is likely. In a first approximation the dimer/trimer disorder can be considered as random but various inter-dimer correlations are probably present, as discussed.

PACS. 61.48.+c Fullerenes and fullerene-related materials – 61.43.Bn Structural modeling: serial-addition models, computer simulation – 78.30.Na Fullerenes and related materials

1 Introduction

The rich pressure-temperature phase diagram of C_{60} exhibits three relatively distinct regions [1–3]. At low temperature ($T < 350$ K), pressure mainly affects the orientation of the C_{60} balls whose molecular structure remains unaltered [4,5]. In an intermediate temperature range (350 K $< T <$ 900 K) double bonds open up on the molecules and a cycloaddition mechanism begins to operate under pressure, leading to polymerized phases with chains or layers of C_{60} molecules linked by four-membered rings [6]. At higher temperature ($T > 900$ K) the C_{60} molecular structure collapses and various phases have been reported, including intriguing ultra-hard disordered or amorphous phases [7,8].

In the intermediate temperature range the first stage of polymerization consists in the formation of C_{60} dimers where pairs of molecules connect via 2+2 cycloaddition. The C_{60} dimers adopt a characteristic dumb-bell D_{2h} symmetry [9,10]. Actually, C_{60} dimers can be obtained using different procedures. Soon after the mass production of fullerenes it was recognized that laser irradiation of C_{60} induces photodimerization [11]. More recently C_{120} has been obtained using a mechanochemical reaction of C_{60} with potassium cyanide [12]. In both cases it was found that the structure of these dimers conforms to that of the high-pressure ones. On the other hand a different dimer structure is observed in the compound $K_2(C_{60})_2$ prepared by solid-state reaction of potassium and C_{60}: in the $(C_{60})_2^{2-}$ anion a single bond joins the two C_{60} molecules [13].

The dimerization of C_{60} thus exhibits various interesting aspects worth studying. This is the case, in particular, of the high-pressure dimers, which can help us understand the mechanisms at play during the first stages of the pressure-induced polymerization. Theoretical and experimental studies have recently addressed the characteristics and properties of these dimers, as summarized below.

Using semi-empirical quantum chemical calculations Ozaki et al. [14] have shown that the dimer is more stable than the monomer and higher polymers and that the distortion of the C_{60} molecules plays an important stabilizing role. Dzyabchenko et al. [15] calculated the possible crystal packings of the C_{60} dimers by minimization of the lattice energy using a bond-charge intermolecular potential model. The authors found that the various packings

[a] e-mail: moret@lps.u-psud.fr
[b] *Present address*: Groupe de Dynamique des Phases Condensées, Université Montpellier II, Place E. Bataillon, CC026, 34095 Montpellier, France

Table 1. Details of the pressure-temperature treatment, lattice parameters and volume per C_{60} for the different crystals.

Crystal number	P-T treatment	Lattice parameter (Å) (±0.05 Å)	Volume per C_{60} (Å^3) (±7 Å^3)
1	1.8 GPa, 450 K for 4 hours	13.77	653
2	$P = 1$ Gpa, $T = 513$ K, 2 h30, followed by $T = 558$ K, 30 min	13.82	660
3	1.5 GPa 423 K, 15 min	13.85	664
4	2.5 GPa, 423 K, 15 min	13.89	670
5	4 GPa, 423 K, 15 min	13.94	677
6	6 GPa, 423 K, 1000 s	13.85	664

retain approximately the C_{60} face-centred cubic arrangement while their relative stability varies with pressure. One of the dimer structures, with symmetry $P2_1/a$, was shown to be geometrically favourable for the formation of the C_{60} polymer chains and of the higher polymers. Experimentally, the X-ray powder diffraction patterns of the dimer state were interpreted in terms of a disordered face-centred cubic (fcc) lattice where each molecule is shifted from its ideal position in the direction of one of its 12 neighbours, i.e. along the $\langle 110 \rangle$ directions, to form a C_{60} dimer [16]. On the average it was found that the cubic fcc symmetry remains. Furthermore, the microscopic structure was suggested to consist of domains (possibly with one of the predicted structures) separated by defects such as stacking faults [16]. However, no experimental evidence for the existence of these predicted structures has been reported, so far.

The spectroscopic (infrared and Raman) properties have been thoroughly examined. Cohesive energy and Raman spectra of the C_{60} dimers have been calculated by Porezag et al. using a density-functional tight-binding method [17]. Detailed comparative studies, by Davydov and co-workers, of the infrared and Raman spectra of the dimer, orthorhombic, tetragonal and rhombohedral phases have been reported [10,16,18,19]. In the Raman spectra clear signatures of the dimers are provided by the shift of the characteristic $A_g(2)$ high energy mode of C_{60} from 1469 cm^{-1} to about 1463 cm^{-1} and the presence of an interball mode at 96 cm^{-1}. The infrared line at 796 cm^{-1} was used to study the kinetics of dimerization of C_{60} at 1.5 GPa and 373–473 K and the dimerization activation energy was determined (134 kJ mol^{-1}) [19]. Far-infrared transmission spectra were measured and calculated using first-principle quantum molecular dynamics for the dimer, linear chain (orthorhombic) and rhombohedral polymers by Long et al. [20]. Wågberg et al. studied the formation of dimers and polymers at 1 and 1.7 GPa using an analysis of the Raman spectra and in particular the $A_g(2)$ peak. The influence of the route through the P-T diagram (isothermal vs. isobaric) and of the orientational state of the C_{60} monomers were analysed [21].

A comparative calorimetric study of the dimers, 1D and 2D polymers, by Iwasa et al. indicated that the dimer state is the most stable and that the stability decreases as the number of intermolecular bonds increases [22]. Thermal expansion of the C_{60} polymers including the dimers was studied between 10 and 500 K by Nagel et al. [23]. Polymerization reduces expansivity, as expected. The depolymerization and its kinetics were also studied between 400–500 K. The activation energies are similar for the dimer and the higher polymers (168 ± 5 kJ mol^{-1} for the dimers) but the depolymerization rate is much higher for the dimers [23].

In spite of the numerous studies devoted to the C_{60} dimers there is a need to collect and analyze more experimental data (in particular structural) to determine the nature of the dimer organization i.e. whether the dimers are ordered and if so what type of structure is stabilized. The analysis of the data is somewhat difficult as spectroscopic and powder diffraction studies [16,19,21,24] have demonstrated that the dimers actually coexists with the monomer and the higher polymers. The details of the pressure and temperature treatment and in particular the path through the P-T diagram, i.e. raising P then T or the opposite, have an effect on the relative proportion of the different polymers. Moreover, the treatment time is an important parameter and the dimers appear to be intermediate products of polymerization [16,19,24]. In fact, it was shown that the maximal content of dimers is about 80–85% in the C_{60} samples polymerized under high pressure and temperature. The possibility of obtaining 100% dimerization thus remains an open question.

In the present work we address some of these problems through combined Raman spectroscopy and X-ray diffraction/diffuse scattering experiments performed on the same C_{60} single crystals. Raman spectroscopy allows us to identify the characteristic modes of vibration of the dimers and other polymers and to analyze the possible phase coexistence. Single-crystal X-ray diffraction/diffuse scattering is adequate for the structural analysis of molecular order/disorder states. The complementarity of these techniques for unravelling fullerene polymer structures was demonstrated previously in the case of the orthorhombic (O′) [25] and tetragonal/rhombohedral (T/R) [26] structures.

2 Experimental

We have studied six C_{60} crystals pertaining to the dimer state. They were prepared according to various experimental procedures and temperature/pressure treatments, as summarized in Table 1.

Crystals 1 and 2 were grown from C_{60} powder (Technocarbo), purified by thermal treatment in a vacuum and sublimated using a two-zone Pyrex-glass vertical oven (700–770 K). The C_{60} monomer crystals were selected by inspection and X-ray diffraction (a minor twin fraction was present in crystal 2). They were compressed in a piston-cylinder device using silicon oil as hydrostatic pressure transmitting medium. Heating was accomplished by inserting the sample in a Pyrex glass tube wound with Kanthal wire. Spun silica wool was used to insulate the oven and reduce temperature gradient and heat losses. The temperature was stable within about 1 K. The treatment was ended by quenching the sample to room temperature under pressure, at an initial rate of about 150–200 K/min, before the pressure was released.

Crystals 3–6 were grown from high-purity (99.98%) fullerite powder (Term USA) by sublimation in a vacuum-sealed quartz tube. The resulting single crystals were taken in hermetic copper tubes containing petroleum oil as hydrostatic pressure transmitting medium. The tubes were treated in a piston-cylinder device "Maxim" (for sample 3) or in a high pressure device "Toroid" (for samples 4, 5, 6). The temperature was stable within about 2 K. At the end of the treatment the crystals were similarly quenched down to room temperature.

The Raman spectra of crystals 1–2 were measured in a back scattering geometry with a Renishaw 1000 grating spectrometer, using a notch filter to remove the Rayleigh line and a CCD detector to collect the Raman scattering. As probing laser we used an Argon ion laser (514 nm). For crystals 3–6 we used a Brucker FT Raman RTS100 spectrometer and a Nd-YAG laser as excitation source (1064 nm). A very low power density (<1 W/cm^2) was employed to avoid inducing any photopolymerization or photo-assisted oxidation. We have observed that single crystals are even more sensitive to such photo-induced effects than are polycrystalline samples.

Diffraction patterns have been collected by taking monochromatic X-ray precession photographs. CuKα (λ = 1.5418 Å) or MoKα(λ = 0.71069 Å) radiations were selected by reflection on doubly-bent graphite monochromators. Details of the scattering patterns up to wave-vectors of about 4 Å^{-1} were obtained using CuKα radiation. Complementary data were obtained with MoKα in order to reach higher wave-vectors in reciprocal space. Both X-ray films (for better spatial resolution and suitability to reveal weak diffuse scattering features) and imaging plates (for rapid collections of digitalised data sets) were used to record the patterns. Precession photographs were made for the main reciprocal planes relative to the cubic lattice of the parent C_{60} monomer phase.

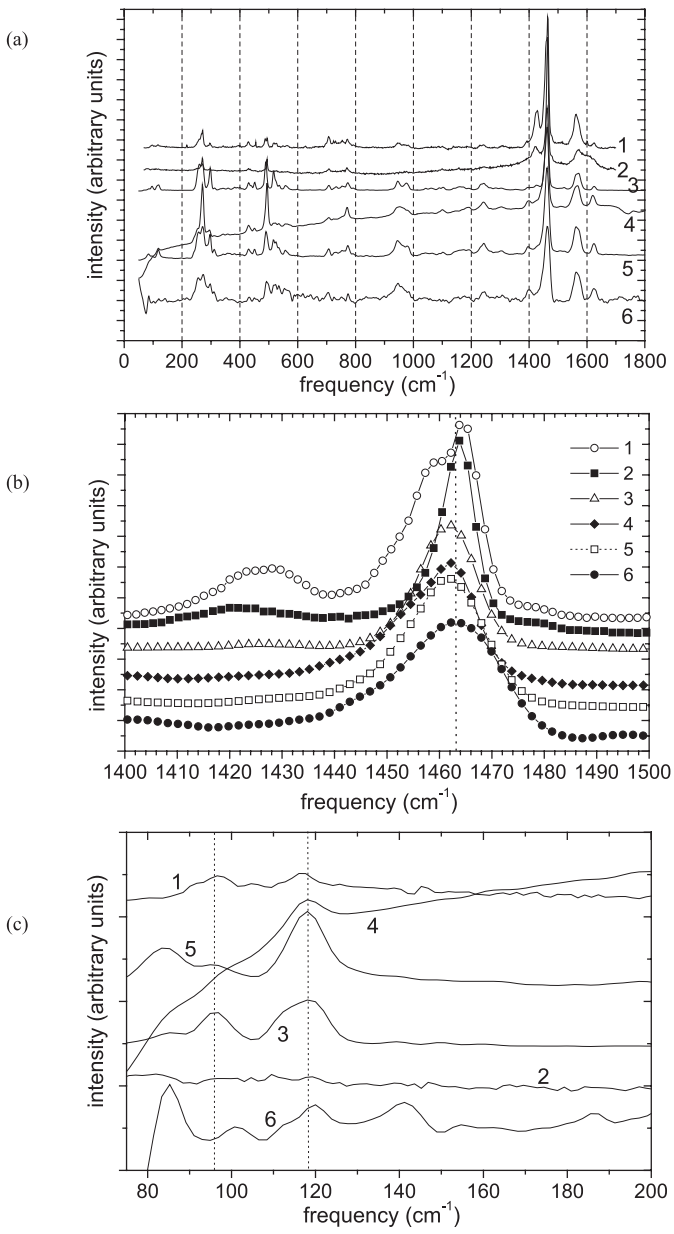

Fig. 1. Raman spectra of crystals 1–6. (a) between ∼70 and 1700 cm^{-1}; the different spectra have been shifted for clarity; (b) between 1400 and 1500 cm^{-1} showing the region of the $A_g(2)$ pentagonal pinch mode, the dotted line marks the frequency (1463 cm^{-1}) associated with the $A_g(2)$ mode for the dimer; (c) low frequency range (<200 cm^{-1}), the dotted lines mark the frequencies associated with the stretching intermolecular mode for the dimers (96 cm^{-1}) and chains (118 cm^{-1}).

3 Results

3.1 Raman spectra

Figure 1 shows the Raman spectra of the 6 crystals studied here. The general appearance of these spectra varies, depending in part on the different technical procedures, such as probing laser and type of spectrometer, used. In particular, different probing lasers can give large differences, especially in the backgrounds of the spectra. In spite of these differences all spectra exhibit similarities in the positions of the main groups of lines. Furthermore, all spectra show the typical signs of polymerization such as a

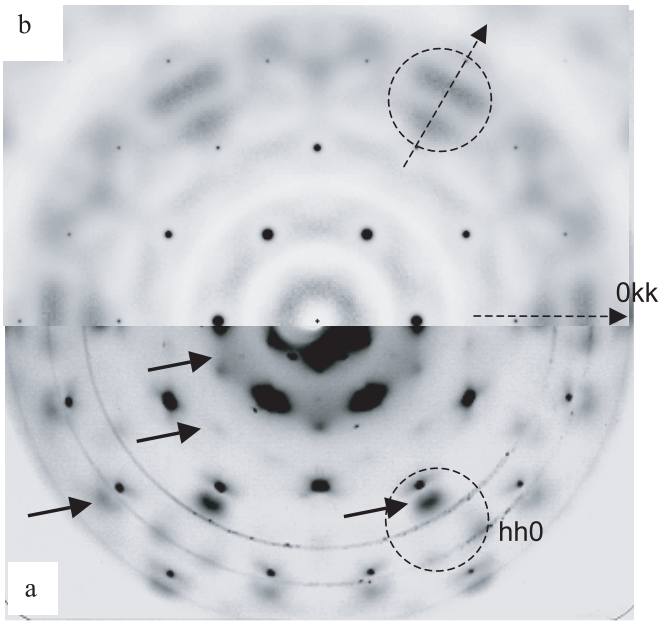

Fig. 2. Diffraction patterns for the $h - k + l = 0$ layer plane (perpendicular to $[1\bar{1}1]$). (a) Experimental precession photograph (CuKα) for crystal 5 and (b) calculated diffraction pattern. In (a) the arrows point to some of the diffuse scattering features. Weak powder diffraction rings are also visible. The dotted circles outline specific regions referred to in the text.

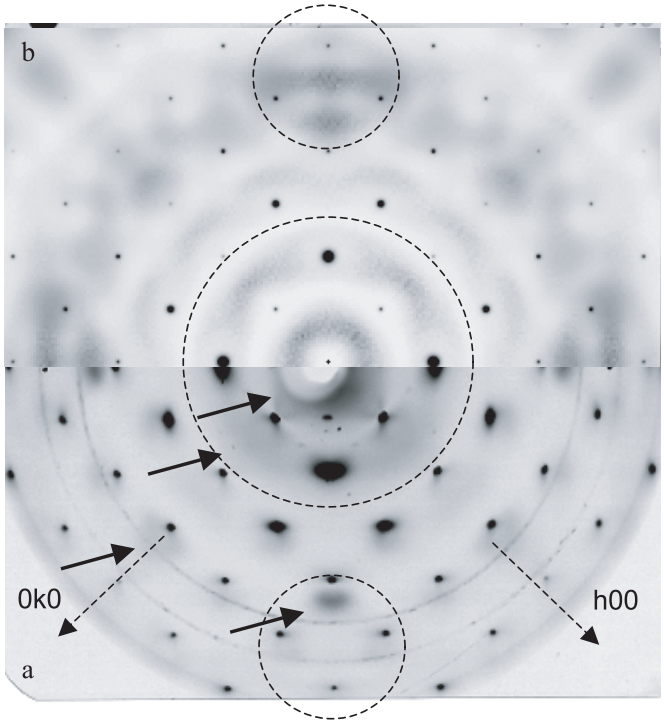

Fig. 3. Diffraction patterns for the $l = 0$ layer plane (perpendicular to [001]). (a) Experimental precession photograph (CuKα) for crystal 1 and (b) calculated diffraction pattern. In (a) the arrows point to some of the diffuse scattering features. Weak powder diffraction rings are also visible. The dotted circles outline specific regions referred to in the text.

splitting of the H_g-modes, a downward shift of the $A_g(2)$ mode, originally at 1469 cm^{-1} (Fig. 1b), and the appearance of new modes. Some of these new modes originate in previously forbidden modes now allowed by the lower symmetry of the molecules formed. The band of modes just below 1000 cm^{-1} and the new modes near 100 cm^{-1} (Fig. 1c) are fingerprints for the existence of covalent intermolecular bonds in the material.

3.2 X-ray diffraction patterns

The high-pressure high-temperature treatments generally preserved the overall shape and cubic symmetry of the crystals (even though the surface morphology of their faces was usually damaged). This cubic symmetry was utilized to orientate the crystals and to collect diffraction patterns (mainly precession photographs) of the main cubic reciprocal lattice planes. This procedure provided us with comprehensive reciprocal space data for all crystals.

Figure 2a shows a typical layer pattern, perpendicular to $[1\bar{1}1]$, (Bragg reflections fulfil the condition $h-k+l = 0$ where h, k, l refer to the cubic lattice) for crystal 5. This pattern exhibits several components:

(i) Bragg peaks corresponding to the cubic lattice (with a unit cell parameter $a = 13.94 \pm 0.05$ Å). They are found to be extinct if h, k and l do not have the same parity, showing that the average lattice is face centred cubic, like the parent monomer lattice at room temperature and atmospheric pressure. These extinctions are fulfilled for all measured patterns (note that some parasitic weak peaks are due to minor twin elements present in the pristine C_{60} crystals; see for example Fig. 7 for crystal 2).

(ii) Diffuse scattering intensity modulations distributed in the entire reciprocal layer. Note, in particular, the broad spots and streaks, marked by black arrows.

These diffraction and diffuse scattering features display the characteristic 6-fold symmetry expected for equatorial layer planes normal to $\langle 111 \rangle$ directions (3-fold axes).

A similar association of Bragg peaks and diffuse scattering modulations is observed for all crystals. As an example, Figure 3a shows the $l = 0$ layer pattern for crystal 1. In this crystal the lattice parameter a is slightly shorter (13.77±0.05 Å). The characteristic 4-fold symmetry is obeyed by both Bragg peaks and diffuse scattering features. Black arrows mark some of the diffuse scattering features.

For the same crystal Figure 4a shows the $l = 0$ layer pattern recorded with MoKα. The pattern reveals the distribution and fading out of the diffraction and diffuse scattering features at high q values.

4 Analysis and discussion of the results

4.1 Raman spectroscopy

The Raman spectra shown in Figure 1 can be analysed on the basis of the detailed knowledge gained from the wealth of theoretical and experimental spectroscopic studies performed in recent years. As compared to pristine C_{60}, the downward shift of the $A_g(2)$ mode from its original position near 1469 cm^{-1} and the splitting of the H_g modes are very clear. The spectra are very similar to those reported previously for the C_{60} dimers obtained by mechanochemical reaction of C_{60} with potassium cyanide [12] and to those observed for the pressure induced dimers [10]. All samples, with the possible exception of crystal 2, show a distinct band of new modes around 980 cm^{-1}. These modes are a clear signature that all samples contain polymer bonds. The very weak band in the spectrum of crystal 2 might indicate that this crystal (or at least its surface) has a lower polymerization level than the others. For the analysis of the Raman spectra of polymeric samples, the $A_g(2)$ line is without doubt the most useful line. Figure 1b shows that this line is centered at 1462–1464 cm^{-1} for all samples, a position which is characteristic for the presence of dimers. For most of the crystals this line is broadened asymmetrically towards lower frequencies, which indicates the presence of a fraction of linear chains contributing their characteristic line at 1459 cm^{-1}. For crystal 1, and to a smaller extent crystal 4, the concentration of such chains is high enough to create a well developed shoulder in the spectrum. Weaker shoulders are also discernible near 1450 cm^{-1} (crystal 4) and 1446 cm^{-1} (crystal 6) indicating a small concentration of 2D polymers. For crystals 1 and 2 one also notes the presence of a mode at about 1425 cm^{-1}, originating from the $H_g(7)$ mode of pristine C_{60}. This mode is often clearly observable when the sample is probed by an Argon ion laser.

The appearance of a low-frequency mode at 96 cm^{-1}, corresponding to longitudinal vibrations in the dimer, is usually taken as another clear signature of the presence of dimers. Figure 1c shows the low-frequency range of the Raman spectra. For crystals 1, 3, 4 and 5 a mode is visible at this position, while it cannot be detected for crystals 2 and 6.

All crystals except crystal 2 clearly reveal a mode at 118 cm^{-1}, a position characteristic for similar vibrations in one-dimensional chains. On the other hand, Figure 1a exhibits a very weak or negligible mode at 344 cm^{-1}. Previous studies have revealed that such a mode is pronounced in the Raman spectra of orthorhombic pressure-polymerized samples [9,27], especially single crystals, but weak or negligible in those of dimer phases or photopolymerized materials [28]. Note, however, that the significance of this mode as a fingerprint of chains and orthorhombic polymers is disputed [18].

In conclusion, the Raman analysis indicates that our crystal samples contain mainly dimers and little unreacted C_{60}. Considering the existence of a shoulder at 1459 cm^{-1} and a weak peak at 118 cm^{-1} observed for most samples we infer a small concentration of short linear chains and higher polymers.

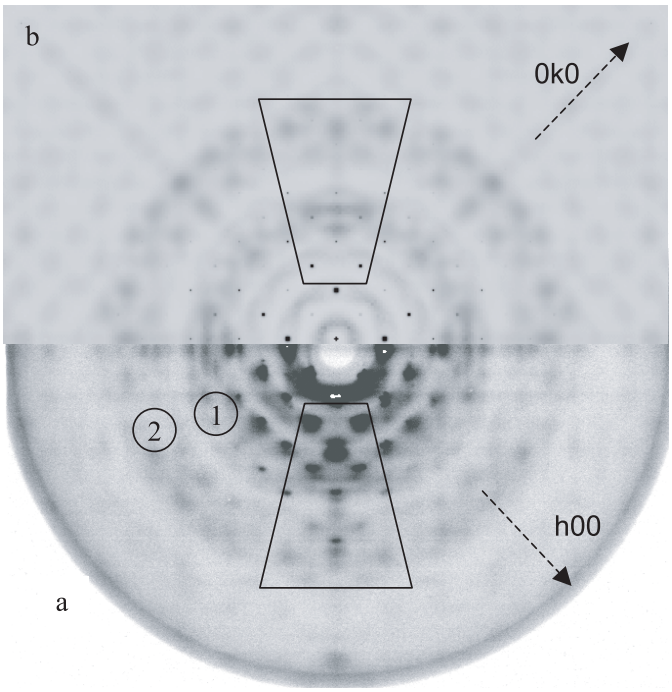

Fig. 4. (a) Precession photograph (MoKα) and (b) calculated diffraction pattern of the $l = 0$ layer plane for crystal 1. Note the relatively good fit in the outlined regions.

4.2 Bragg peaks and diffuse scattering

The Bragg peaks correspond to the average structure of the dimer state while the diffuse scattering intensity is the signature of structural disorder i.e. unit-cell dependent deviations from this average structure.

The average structure can be described within a face centred cubic lattice and there is no signature of other structures such as the 1D orthorhombic phases (O and O′) or the ordered dimer structures predicted by Dzyabchenko et al. [15] (for instance the monoclinic $P2_1/a$ structure). From the sets of precession photographs obtained for all crystals studied here (1–6) we have derived cubic unit-cell parameters, which are listed in Table 1, together with the corresponding volumes per C_{60} unit (1/4 of the unit-cell volume). On average the cell parameters are about 2% shorter than that of the ambient pressure C_{60} monomer (14.15 Å). In fact, the volumes per C_{60} are close to that of the "low pressure" orthorhombic polymer phase (O′) as found by Moret et al. (663 $Å^3$) [25] and Agafonov et al. (658 $Å^3$) [29] and slightly larger than that of the "high pressure" orthorhombic polymer phase (O) reported by Núñez-Regueiro et al. (650.5 $Å^3$) [30,31]. We point out that the unit-cell parameter values for the 6 crystals do not exhibit a clear dependence on the pressure and/or temperature of the treatment. On the other hand they are spread slightly more than expected from

the estimated accuracy of the measurements. This may reflect some difference in structural organization (the disorder model proposed below in Sections 4.3 and 4.5 is flexible; the degree and nature of disorder may vary, in relation with the details of the P-T treatment). Note that in Figures 2a and 3a, for instance, the Bragg peaks at low-q values appear to be broad, in particular in the azimuthal direction. This effect can be attributed, for the most part, to the combination of a saturation of the photograph with the large mosaic spread of the crystals (another possible contribution will be mentioned below, in Sect. 4.4).

Turning to the diffuse scattering we first recall that C_{60} crystals (monomer) are known to produce two broad spherical halos of diffuse scattering intensity at $q_1 = 3.3$ Å^{-1} and $q_2 = 5.3$ Å^{-1}. This diffuse scattering originates from the orientational disorder of the C_{60} cages rotating about their centres. The intensity within the halos is continuous but it displays modulations whose analysis has given information on the nature of the intermolecular interactions (see [32] for a review). The diffuse scattering observed for the present crystals exhibits some similarities with that of the C_{60} monomers. Figures 2 and 3 and in particular Figure 4a show that the intensity of the diffuse scattering features is maximum inside 2 circular regions (labelled 1 and 2 in Fig. 4) corresponding to the monomer halos, at $\sim q_1$ and q_2. Actually, this can be attributed to the properties of the C_{60} molecular structure factor, related to the shape of the molecule (using the symmetry-adapted-function formalism this structure factor can be expanded in terms of spherical Bessel functions and it exhibits maxima around q_1 and q_2, as shown previously [32–34]). However, the distribution of diffuse scattering intensity maxima and modulations (Figs. 2–4) is markedly different from those of the C_{60} monomer [35,36]. The absence of "monomer halos", as such, establishes that the fraction of orientationnally disordered C_{60} monomers in the present crystals is too small to produce an observable diffuse scattering intensity. We can roughly estimate that the concentration of monomers is less than 10–15%. This is in agreement with the analysis of the Raman results (Sect. 4.1).

4.3 Structural model of disordered dimer lattice

On the other hand, as the Raman data indicate that the crystals contain a large amount of dimers it is reasonable to assume that the observed diffuse scattering is the signature of some disorder introduced in the monomer crystal structure upon the formation of dimers. This should be considered in relation with the dimerization mechanism. A reasonable assumption is that C_{60} monomers are drawn closer by pressure and undergo thermally activated librations so that C_{60} pairs may happen to be in favourable orientations to join via the opening of facing double bonds on each molecule and the formation of four-membered rings. In a first approximation one can consider that this process is random: in the face-centred cubic monomer structure the bonding of near-neighbour C_{60} molecules proceeds randomly. In particular the dimers form along any of the 6 equivalent $\langle 110 \rangle$ directions. Therefore, the disorder of the C_{60} dimers should exhibit both positional and orientational character.

To test this hypothesis we have built a structural model for the disordered dimer lattice and the resulting Bragg peak and diffuse scattering intensities have been calculated. We consider a C_{60} model crystal of dimensions $N_1 \times N_2 \times N_3$ unit cells and we use a random choice algorithm to select a C_{60} molecule. If this molecule is a monomer, i.e. not engaged in a dimer yet, we select at random one of its monomer near-neighbours (excluding the C_{60}'s already dimerized) and the corresponding C_{60} pair is formed by drawing the molecules closer by $\delta/2$, symmetrically, along the $\langle 110 \rangle$ direction. δ ($\sim$0.69 Å) is the difference between the C_{60}-C_{60} distance in a fcc monomer lattice with parameter 13.85 Å (the average parameter for the present crystals) and the C_{60}-C_{60} distance, i.e. 9.10 Å [12,37] for a dimer molecule. This procedure is repeated until no new dimer can be formed (details are presented in Appendix A). It should be noted that it is not possible to obtain 100% dimerization using such a procedure and a small fraction (about 3.5%) of C_{60} monomers are "trapped" because all their neighbours are already dimerized.

Figure 5 displays a representative section of the corresponding 3D model crystal showing the distribution of the dimers formed by the molecules in one arbitrary (001) layer.

A supplementary source of disorder lies in the orientation of the dimers around their respective $\langle 110 \rangle$ axes as defined, for instance by the orientation of the plane formed by the four-membered ring. In a first approach we have assumed that this orientation is randomly distributed within the crystal either dynamically if the dimers rotate or librate around their axes or in a frozen configuration. However, inter-dimer interactions are not negligible completely and correlations should certainly be introduced in a more accurate description of the dimer organization.

4.4 Comparison of experimental and calculated diffraction patterns

We have calculated the Bragg peak and diffuse scattering intensities produced by the above model crystal characterized by i) dimers randomly distributed in position and $\langle 110 \rangle$ orientation, ii) complete rotational disorder of the dimers around their $\langle 110 \rangle$ axis. Details of the calculation are given in Appendix B.

To probe the validity of the model the calculation has been used to simulate the experimental diffraction patterns and in particular those of Figures 2a, 3a and 4a, for the layers defined by $h + k + l = 0$ and $l = 0$. The experimental Bragg peak intensities are semi-quantitatively reproduced by the calculation. Calculated Bragg peak intensities are only slightly different for crystals formed of monomers, dimers (+ monomers) and trimers (+ monomers), as is illustrated in the case of dimers and trimers in Figures 7a and 7b. Moreover, the

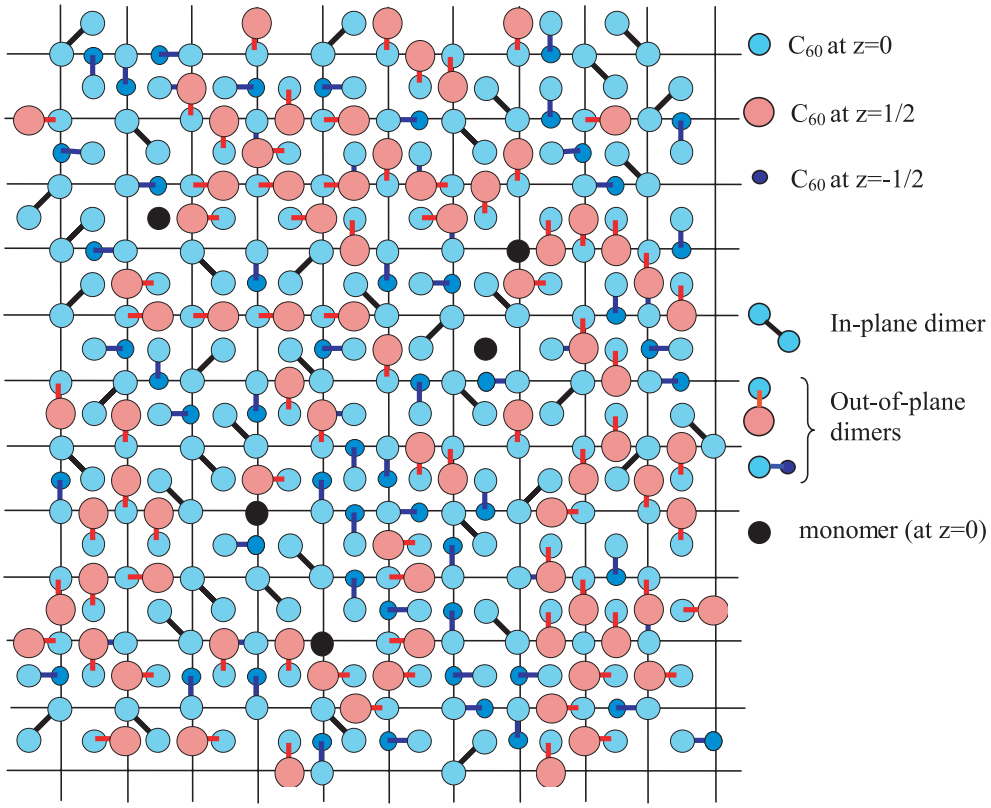

Fig. 5. Distribution of the C_{60} dimers (and remaining monomers) in a (001) plane of the model crystal. In-plane and out-of-plane dimers involving, at least, one C_{60} molecule located in the (001) plane are represented.

complete rotational disorder approximation used (see Appendix B) may be a too crude approximation to account precisely for Bragg peak intensities [32,38]. The broadening of the low-q Bragg peaks observed in Figures 2a and 3a was attributed in Section 4.2 to a combination of saturation and mosaic spread. We mention here that it may also partly reflects some deviation from the average lattice model that is considered here. We do not analyse in details the Bragg peak intensities in this paper, but we put emphasis on the distribution of the diffuse scattering intensity, which provides a more stringent test. Note that the Bragg peak and diffuse scattering intensities calculated in Appendix B have different scales. Therefore, in Figures 2–4, 6 and 7 the relative weights of the Bragg and diffuse scattering components have been normalised to match the observed patterns.

Figures 2b, 3b and 4b show simulated diffuse scattering patterns to be compared with the corresponding experimental ones. Based on visual inspection it appears that the agreement between the experimental and simulated diffuse scattering distributions is qualitatively satisfactory in several regions. To test the dependence of the diffuse scattering intensity distribution on the intermolecular distance d of the dimer we have calculated the diffraction patterns for different values of d (or δ). Figure 6 shows a set of $h-k=0$ calculated patterns for $d=9.79$, 9.45 and 9.10 Å ($\delta=0, 0.34$ and 0.69 Å, respectively) together with the corresponding experimental pattern obtained for crystal 2. The main effects of varying the d value can be summarized as follows. In the case of the monomer distance ($d=9.79$ Å) no diffuse scattering is observed at low angle. As d is shortened some diffuse scattering develops in this region. Moreover the diffuse scattering maxima move slowly outwards (to higher q values, see for instance the row of diffuse spots outlined in the figures). The sensitivity of these effects is obviously not high enough so that it could be used to determine the intermolecular distance d but it appears that the value chosen here to simulate the patterns of Figures 2–4 (9.10 Å) is quite satisfactory.

The qualitative agreement of the experimental and simulated diffuse scattering distributions strongly suggests that the present model of randomly disordered dimers constitutes a rather good approximation for the structure of our crystals. However, several discrepancies remain, at the quantitative level, in particular when the relative intensities of the various diffuse scattering modulations are considered. This is the case for instance in the region of the (forbidden) (550) reflection (circled in Figs. 2 and 3) where the experimental and simulated diffuse scattering exhibit differences. In Figure 3, the central region of dark and light diffuse scattering (circled in dotted line) is not reproduced adequately. These discrepancies indicate that the model could be improved or refined. Some suggestions along these lines are discussed below.

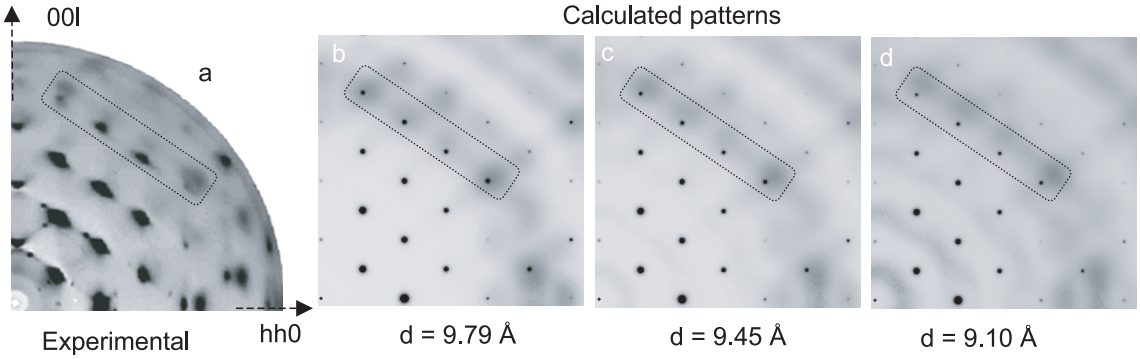

Fig. 6. (a) Experimental (CuKα, crystal 2) and (b-d) calculated diffraction patterns of the $h-k=0$ layer plane (perpendicular to $[1\bar{1}0]$) for different values of the intermolecular distance of the dimers.

4.5 Proposed improvements of the structural model

Firstly, even though the dimers appear to dominate, the Raman results suggest that a small fraction of other polymers are formed. Furthermore, several IR, Raman and X-ray diffraction studies have shown that a mixture of dimers, 1D chains (orthorhombic phases) and 2D polymers is often observed in the low-pressure low-temperature region [18,19,21]. This prompted us to investigate the possibility of C_{60} trimers, which are the first stage leading from dimers to short chains. To test this hypothesis we have built a randomly disordered structural model with trimers using a similar algorithm as for the dimers (see Appendix A). This procedure leads to a maximum concentration of 87% of trimers and 13% of monomers. The calculated diffuse scattering produced by this model is shown in Figure 7a for the $h-k=0$ layer plane. Figure 7b shows the corresponding diffuse scattering produced by the disordered dimer model described in Section 4.3. Overall the two distributions are similar and the intensity maxima are located in the same regions but the trimer model generates a sharper diffuse scattering distribution (as expected, qualitatively, if one considers that trimers form a more "correlated" model than the dimers). Comparing with the experimental pattern (crystal #2, Fig. 7c), it appears that this "sharpening effect" leads to some improvement of the fit, in particular at large q values where the observed diffuse scattering modulations are sharper than those of Figure 7b. However, at low q's, the peculiar pattern of undulating streaks of the trimer model (Fig. 7a) is not observed experimentally. Note also that, near the (550) reflection (dotted circles) the diffuse scattering intensity distribution is still different from the experimental one. Therefore, it appears that the model of disordered trimers leads to some improvement of the fit, even though it is limited. It is thus reasonable to consider that a small fraction of disordered trimers (and probably short chains) are present in the low-pressure low-temperature region.

The algorithm we used to build the model implies that, once a dimer (trimer) is formed, the two (three) corresponding molecules cannot pair with another molecule. This intrinsic "exclusion" scheme induces occupational correlations for the formation of the neighbouring dimers (trimers). Moreover, other types of correlations between

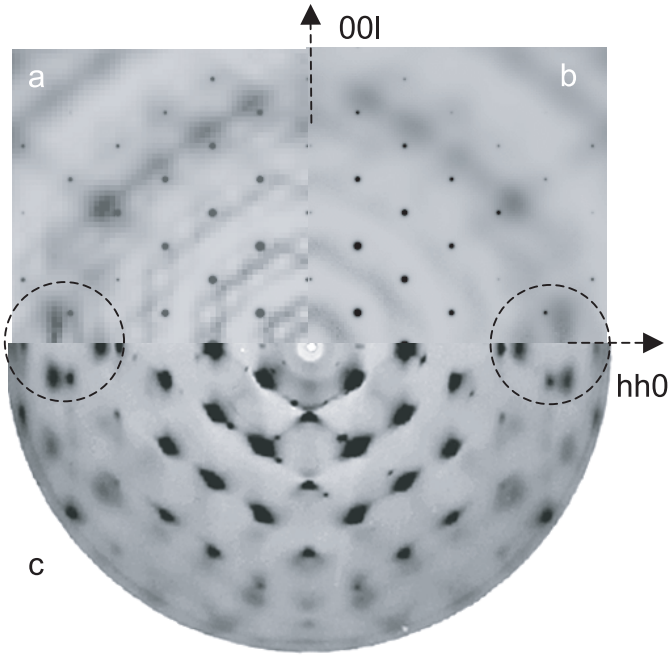

Fig. 7. Diffraction patterns for the $h-k=0$ layer plane (perpendicular to $[1\bar{1}0]$). The diffuse scattering distributions calculated for (a) the disordered trimer model and (b) the disordered dimer model are compared to the (c) experimental pattern (CuKα, crystal 2). The dotted circles outline specific regions referred to in the text.

neighbouring dimers (or trimers) are worth considering. In particular, the formation of a dimer leads to a displacement of two C_{60} molecules which modifies the local environment of their neighbours. As a result the further dimerization of neighbouring C_{60} molecules will be influenced. It may be favoured, leading to a clustering of dimers, or hindered. This will affect also the orientation of the dimers to be formed. For instance, there may be a tendency to form parallel dimers, i.e. with the same specific $\langle 110 \rangle$ axis. Such an alignment would be favourable to the formation of ordered chains as found in the orthorhombic polymer structures. The influence of this type of correlations (i.e. a tendency for the alignment of dimers) on the

diffuse scattering has not been investigated in the present work.

Apart from simply aligning, the dimers could adopt more elaborate arrangements such as the ordered structures proposed by Dzyabchenko et al. [15]. We already mentioned above that the Bragg peaks (average structure) did not show evidence for these ordered structures which means that they are not stabilised at long-range. However similar configurations could be stabilised locally in the form of short-range correlations. It would be useful to introduce these correlations in the structural model and to test their effects on the diffuse scattering.

One should also consider the specific orientation of the dimers about their axis. In the above model we have assumed full orientational disorder around their axis (static or dynamic). This is clearly a simplification because dimer-dimer and dimer-monomer interactions should influence the orientation of the dimers around their axes. Preferred orientations should occur and affect the diffuse scattering intensity distribution.

Introducing these various types of interactions into the structural model would be a challenging but rewarding task as it would help us understand the mechanisms of the transition from the dimers to the higher oligomers. In this respect, a comparison of the calculated and experimental diffuse scattering intensity should be a well-suited probe to discriminate between the various models of interactions.

5 Discussion and conclusion

Our results show that C_{60} crystals predominantly formed of disordered dimers (with minor fractions of monomers, trimers, chains and 2D polymers) can be prepared in a relatively wide pressure range. This is in agreement with previous pressure-temperature diagrams of C_{60} (see [18] for example). Figure 8 displays a tentative updated diagram, for the low-P low-T ranges, that combines recent results [16,18,19,21,24]. The two shaded regions (with approximate contours) mark the zones of appearance of the dimers, in coexistence with the monomer, trimers, 1D and 2D polymers. Note that dimerization has been found to start at room temperature already [24]. Labels 1–6 mark the present crystals. crystal 2 (1 GPa, 558 K) stands at the low-P border of the upper region while the points representing the other crystals are located near the (tentative) limit separating the two regions. We have also included data points for the orthorhombic O′ structure observed in crystals treated at 1 GPa-585 K [25] and 1.5 GPa-723 K [29].

As we pointed out already (Sect. 1) the path used to establish the pressure-temperature conditions and the treatment time affect the resulting states of polymerization This is the case in the shaded regions but it is also true for the 2D polymers. Thus, the "heating then pressing" procedure leads to predominantly tetragonal $P4_2/mmc$ structures (where the successive polymer sheets are rotated by 90°) [26,39] while "pressing then heating" was found to stabilize a different stacking (Immm), all layers having the same orientation [40]. It is also worth noting that powders and single-crystals may lead to different polymerized states when treated under similar conditions. This is indicated, for example, when comparing crystal 2 with a powder sample treated under the same conditions by Wågberg et al. [21]. While crystal 2 is composed essentially of dimers the powder was found to contain about 55% chains (linear and branched) and only 27% dimers. The fact that powders appear to polymerize more "easily" than macroscopic single crystals may be a size effect if we assume that the relatively slow rearrangements needed to obtain aligned and ordered polymer chains (and layers) from the disordered dimers (see below) are more efficient in very small crystallites. Interestingly, it was shown that a single crystal treated at 585 K (instead of 558 K) and the same pressure (1 GPa) is almost completely composed of polymerized chains (orthorhombic structure O′ [25]): a slightly higher temperature seems to be required for single crystals.

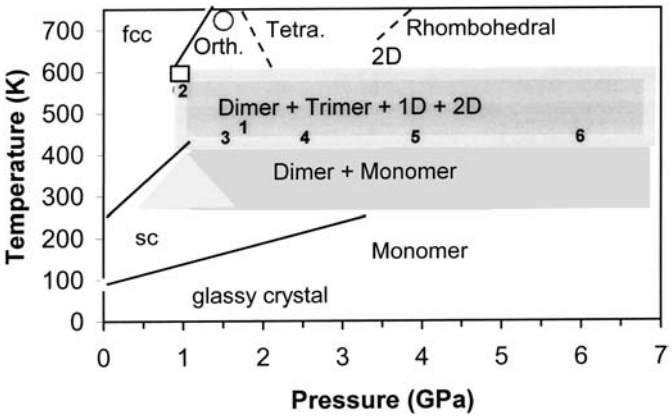

Fig. 8. Tentative pressure-temperature diagram of C_{60} in the low-P low-T region. The monomer phases (fcc, sc and glassy crystal) are separated by solid lines. Two shaded regions denote the coexistence of different structures. The dashed lines separate the stability regions of the orthorhombic, tetragonal and rhombohedral structures. The numbers stand for the 6 crystals studied here while the square and circle correspond to orthorhombic crystals (structure O′) treated at 1 GPa–585 K [25] and 1.5 GPa–723 K [29], respectively.

The influence of the pressure/temperature treatment on the structure of the polymerized states should be considered in relation with the structural properties of the specific monomer phase (face-centred-cubic or simple-cubic) that serves as a "parent" phase. The stability regions of these two phases, separated by an ascending line, are shown in Figure 8.

At $P = 1$ GPa, as the temperature is raised (for instance to 558 K as for crystal 2), the formation of the dimers proceeds inside the fcc monomer phase region, where the C_{60} molecules undergo rapid reorientations about their centers. It implies a high probability for C_{60} neighbours to align two of their 30 double bonds and join via the opening and condensation of these bonds into four-membered rings. For the other crystals (1, 3–6) the dimerization is achieved inside the sc region where the orientations of the C_{60} molecules are such that electron-rich

double bonds face either electron-poor pentagons (P orientation) or hexagons (H orientation). In fact, while the P orientation is more stable at low pressure and low temperature, the H orientation is rapidly stabilized by pressure (see [2] for a review) so that the dimerization of crystals 1 and 3–6 is achieved with H-oriented molecules. It has been shown that small librations about the H orientations are sufficient to bring neighbouring molecules into adequate bonding orientations [31].

It has been suggested that the higher degree of orientational disorder of the fcc phase would lead to less well ordered polymers than the sc phase. In particular, the low-pressure polymers and the photo-polymers would be more disordered than the high-pressure polymers [31]. Our results actually show that whatever the "parent" phase, fcc or sc, dimerization appears to generate dimers which are disordered both positionally and orientationally (Sect. 4.4). No ordered arrangement of the dimers is stabilized at long-range; the dimers form randomly along any of the six equivalent $\langle 110 \rangle$ directions and their orientation about the dimer axis is (in a first approximation) arbitrary.

The disordered dimer state, as represented for instance by our model structure in Figure 5, raise questions about the further stages of polymerization. The formation of parallel polymer chains, such as in the O and O$'$ orthorhombic structures, requires numerous rearrangements (breaking intermolecular dimer bonds – four-membered rings – and forming new ones). As the temperature is raised and the chains become more stable these rearrangements have to become cooperative in order to lift the frustration of the disordered dimer structure. A likely possibility is that the strains induced by the molecular displacements (shortening of the intermolecular distance as a result of the bond formation) probably favour polymerization in a directionally ordered process, as pointed out by Wågberg et al. [21]. At 1 GPa, for example, this cooperative process leads to the formation of the O$'$ structure between 558 and 585 K [25] with little remaining disorder, except for the presence of domains due to the six equivalent $\langle 110 \rangle$ directions of the chains and the associated cubic-orthorhombic symmetry lowering.

Turning to the formation of the 2D polymers from either the O or O$'$ structures, which implies the combination of parallel chains into layers we emphasize that it can be achieved by specific rotations of these chains (around their axes) to allow for interchain bonding, without breaking the chains, as pointed out earlier [41]. We recall that, in the orthorhombic structures, the orientations of the chains (around their axis) are either identical ($\mu = 0°$, O structure) or alternate ($\mu \sim \pm 29°$, O$'$ structure) (as usual the chain orientation is defined by the angle μ formed by the plane of the four-membered ring and the ($\mathbf{a}$, $\mathbf{c}$) orthorhombic plane). To obtain the tetragonal $P4_2/mmc$ structure, for instance, further rotations of the chains are needed so that the orientation of chains belonging to successive layers are alternatively parallel ($\mu = 0°$) and perpendicular ($\mu = 90°$) to the stacking direction (see Fig. 1 in Ref. [41]).

Finally it is worth comparing the characteristics of the dimerization and polymerization in C_{60} and in C_{70}. Lebedkin et al. [42] studied in details the dimerization of C_{70} at 1 GPa and 450 K and they found that the molecules join by [2+2] cycloaddition across double bonds from the polar regions to form four-membered rings, in a similar way as for C_{60}. This dimerization is favoured by the parallel orientation of the molecular 5-fold axes and the uniaxial rotation about these axes. Strong similarities between C_{60} and C_{70} dimers have been reported (spectroscopic properties, thermal and photodissociation) but an interesting difference is that, while C_{60} dimers can be considered as an intermediate state of the polymerization process (with treatment time being an important parameter), the dimerization of C_{70} appears to be "kinetically" frozen [42]. On the other hand the structural organization of the C_{70} dimers has not been characterized but it is likely that they are disordered, at least partially. A diffraction/diffuse scattering study similar to the present one would give information on this question. We note that a C_{70} molecule can bond to several neighbours, up to 12, like in C_{60}, but there are only 10 reactive double bonds per molecule instead of 30. This may cause a more frustrated situation for the C_{70} dimers when they rearrange in order to form chains. This has been actually achieved, at higher pressure and temperature (2 GPa, 573 K) by Soldatov et al. who were able to polymerize C_{70} single crystals (with hexagonal-close-packed stacking) and obtained zig-zag linear chains aligned in an orthorhombic structure [43].

In conclusion, the combination of Raman spectroscopy and X-ray diffraction/diffuse scattering on high-pressure high-temperature treated C_{60} single-crystals has allowed us to characterize the C_{60} dimers. Although the dimer state is an intermediate product of polymerization all 6 crystals, prepared in the range 1–6 GPa, are composed, for the most part, of dimers, with minor fractions of monomers, 1D and 2D polymers. In the whole pressure range the dimers are disordered and the associated diffuse scattering intensity distribution has been analyzed using computer-generated model structures. By comparison of the diffuse scattering produced by these model structures with the observed single crystal scattering patterns we have shown that the dimers are both positionally and orientationally disordered. Calculations were also made for similar model structures based on trimers indicating that a small concentration of disordered trimers probably coexist. In a first approximation the dimer/trimer disorder can be considered as random although inter-dimer/trimer correlations are likely.

J.M. Godard and N. Blanchard are acknowledged for the growth of C_{60} single crystals. M. Gabay is thanked for interesting discussions on disorder models. The present work was supported by the Russian Foundation for Basic Research (Grant 03-03-32640) and NATO Science Program (Grant PST.CLG.979714).

Appendix A: Structural model of disordered dimer and trimer lattices

We consider a face centred cubic crystal of C_{60} molecules, formed of $N_1 \times N_2 \times N_3$ unit cells. Its unit cell parameter a is chosen as that of the average lattice found for the dimer state: $a \sim 13.85$ Å. It consists of four simple cubic sub-lattices and thus contains $4 \times N_1 \times N_2 \times N_3$ molecules. This crystal is placed inside a larger box formed of $(N_1+2) \times (N_2+2) \times (N_3+2)$ unit cells, to avoid spurious effects at its borders. We associate to each molecule a three-dimensional vector '**u**' that will define the molecular displacement associated with the dimerization.

Let us first detail the procedure developed to obtain a crystal of dimers. We use a random choice algorithm to select a C_{60} molecule among the $4 \times N_1 \times N_2 \times N_3$ molecules of our crystal. We select at random one of its twelve near-neighbours (even if the molecule is at the border of the crystal, all twelve-neighbours can be considered because of its inclusion in a larger box). These two selected molecules are then associated to form a dimer. The displacement associated to the first molecule is set to $\mathbf{u} = \delta\mathbf{R}/\sqrt{2}$ and that associated to the second one is $\mathbf{u} = (-\delta)\mathbf{R}/\sqrt{2}$, where $\mathbf{R}$ is the intermolecular distance in the monomer crystal, in reduced units (along $\langle 110 \rangle$ direction, $\mathbf{R}$=(1/2,1/2,0) for instance). In the dimer, the molecules are thus displaced by $\delta/2$ one toward the other, and the intermolecular distance is $d = \frac{a}{\sqrt{2}} - \delta$. For $a = 13.85$ Å and $d = 9.1$ Å [12,37], the displacement δ is 0.69 Å.

We then consider the smaller set of molecules formed of those not yet selected before: there are $(4 \times N_1 \times N_2 \times N_3 - 1)$ such molecules if the second selected molecule was outside our crystal, or $(4 \times N_1 \times N_2 \times N_3 - 2)$ otherwise. The above selection process of a pair of molecules is repeated within this smaller set (the second molecule of the pair being chosen, at random, among the monomers which are nearest-neighbours of the first selected molecule).

This procedure is iterated until all molecules have been taken under consideration. It allows us to construct a crystal formed of dimers with no correlations between their long axes orientations and their positions, as is illustrated in Figure 5. A small amount of monomers still remains: it happens when all neighbours around a selected molecule are already belonging to a dimer. Typically, with our procedure, the amount of trapped monomer molecules is about $m = 3.5\%$.

The procedure used to obtain a crystal made of trimers (with no correlations between their long axes orientations and their positions) is very similar to the one developed above for the dimers. A molecule is chosen at random as above. We then consider the pairs of nearest neighbours on each side of this molecule, which can bond to it and form a trimer (meaning that none of the neighbours is already involved in a trimer). A pair of nearest neighbours is then chosen at random among the available pairs. The central molecule is characterized by a displacement $\mathbf{u} = \mathbf{0}$, the two others have displacements $\mathbf{u} = 2\delta\mathbf{R}/\sqrt{2}$ and $\mathbf{u} = -2\delta\mathbf{R}/\sqrt{2}$, $\mathbf{R}$ being an intermolecular distance in reduced units, as above. The distance between molecules in the trimer is the same as in dimers: $d = \frac{a}{\sqrt{2}} - \delta$. Some monomers remain, with $\mathbf{u} = \mathbf{0}$, when no pair of neighbours can be selected to form a trimer. This restriction on a pair of neighbours being more severe than that on a single neighbour used for dimers, the amount of monomer molecules is larger: $m \sim 13\%$.

Appendix B: Calculation of the Bragg peaks and diffuse scattering intensities for the structural models

In the dimer or trimer model crystals, the n-mers long axes orientations and positions are not correlated and the monomers are randomly located. On average, the positions of the molecules are those of the initial crystal. The crystal thus exhibits an average face-centred cubic symmetry with unit cell parameter a, as observed experimentally. The disorder due to the dimers or trimers random orientations and to the dimers or trimers and monomers random relative positions gives rise to specific diffuse scattering.

To calculate the scattered intensity, we make summations over the $4 \times N_1 \times N_2 \times N_3$ molecules positions in the starting monomer crystal or in the resulting dimerised or trimerised ones: for a molecule M, the initial position is $\mathbf{R}_\mathrm{M}$ and the final one $\mathbf{R}_\mathrm{M} + \mathbf{u}_\mathrm{M}$, where $\mathbf{u}_\mathrm{M}$ is the displacement $\mathbf{u}$ associated with each molecule (see Appendix A). We assume that C_{60} monomers have random orientations with respect to their centres of mass, and that molecules in C_{60} dimers or trimers form a rigid set, which can take any orientation with respect to the n-mer long axis. No positional Debye-Waller factor is considered in this first approximation. In the following, one will calculate rotational mean values of molecular form factors or of products of them '$\langle .. \rangle_\mathrm{rot}$' within the scope of this hypothesis.

The scattered intensity $I(\mathbf{q})$, where $\mathbf{q}$ is the wave vector, writes

$$I(\mathbf{q}) \sim \sum_{\mathrm{M},\mathrm{M}'} \langle F_\mathrm{M} F^*_{\mathrm{M}'} \rangle \exp(i\mathbf{q}(\mathbf{u}_\mathrm{M} - \mathbf{u}_{\mathrm{M}'})) \exp\left(i\mathbf{q}(\mathbf{R}_\mathrm{M} - \mathbf{R}_{\mathrm{M}'})\right).$$

It can be expressed as the sum of two terms: $I_\mathrm{B} + I_\mathrm{D}$, with

$$I_\mathrm{B}(q) \sim \langle F_\mathrm{M} \rangle \langle \mathrm{F}^*_{\mathrm{M}'} \rangle \langle \exp(i\mathbf{q}(\mathbf{u}_\mathrm{M} - \mathbf{u}_{\mathrm{M}'})) \rangle \times \sum_{\mathrm{M},\mathrm{M}'} \exp(i\mathbf{q}(R_\mathrm{M} - R_{\mathrm{M}'}))$$

$$I_D(\mathbf{q}) \sim \sum_{\mathrm{M},\mathrm{M}'} \left(\langle F_\mathrm{M} F^*_{\mathrm{M}'} \rangle \exp(i\mathbf{q}(u_\mathrm{M} - \mathbf{u}_{\mathrm{M}'})) - \langle F_\mathrm{M} \rangle \langle F^*_{\mathrm{M}'} \rangle \times \langle \exp(i\mathbf{q}(\mathbf{u}_\mathrm{M} - \mathbf{u}_{\mathrm{M}'})) \rangle \right) \exp(i\mathbf{q}(\mathbf{R}_\mathrm{M} - \mathbf{R}_{\mathrm{M}'})).$$

The first term gives Bragg peaks, associated with the average lattice, while the second one corresponds to diffuse scattering, i.e. disorder or local order with respect to the average lattice.

Table 2. Parameters used to calculate the form factor of a C_{60} molecule averaged over its rotation around an axis of polymerization i. The molecule can be decomposed into layers j at abscissa z_j Å along the axis (the origin is at the centre of the molecule). In a layer j, $n(j)$ C atoms are located on a circle of radius R_j (Å).

j	z_j	R_j	$n(j)$
1	0	3.54	4
2	0.72	3.47	12
3	1.17	3.34	8
4	1.42	3.24	8
5	2.30	2.69	8
6	2.59	2.41	8
7	3.02	1.85	8
8	3.47	0.70	4

The molecular form factors and their products, averaged over orientational disorder, are given below.

The form factor of a C_{60} monomer, averaged over all its orientations, is given by

$$\langle F(q)\rangle_{\text{orientations}} = 60 f_c(q) j_0(qR)$$

where j_0 is the spherical Bessel function of order 0, fc is the form factor of carbon, q is the modulus of the wave-vector $\mathbf{q}$ and R is the C_{60} molecule radius ($R \sim 3.54$ Å).

For a molecule rotating around an axis i ($i = 1$–6 correspond to the six near neighbour directions: [110], [1$\bar{1}$0], [011], [01$\bar{1}$], [101], [10$\bar{1}$]), the form factor writes

$$\langle F(\mathbf{q})\rangle_{\text{axis } i} = f_c(q) \sum_{j=1}^{8} n(j) \cos(q_{\parallel}(i) z_j) J_0(q_{\perp}(i) R_j)$$

where $\mathrm{q}_{\parallel}(i)$ and $q_{\perp}(i)$ are the components of the wave vector $\mathbf{q}$ along the direction i and perpendicular to it. The index j runs over layers of atoms on the C_{60} molecule perpendicular to the axis i, with $z_j \geq 0$, z_j being the layer abscissa along i. R_j is the distance of C atoms in layer j to the axis i and $n(j)$ is the number of atoms in layers of abscissa $\pm z_j$. Values of z_j, R_j and $n(j)$ are given in Table 2. J_0 is the cylindrical Bessel function of order 0.

The mean value of the product $\langle F_{\mathrm{M}} F^*_{\mathrm{M}'} \rangle$ is equal to the product of the mean values $\langle F_{\mathrm{M}} \rangle$ and $\langle F^*_{\mathrm{M}'} \rangle$ if M $\neq$ M′ or if M and M' do not belong to the same n-mer. Indeed, in this case, the molecular orientations are not correlated.

For M= M'= monomer, using the symmetry adapted function formalism [32–34], one calculates

$$\langle F(\mathbf{q}) F^*(\mathbf{q})\rangle_{\text{iso}} = 4\pi f_c^2 \sum_{l=6,10,12,16,18\ldots} (g_l j_l(qR))^2$$

where $g_6 = 2.56$, $g_{10} = 19.35$, $g_{12} = 7.89$, $g_{16} = 17.9$, $g_{18} = 38.2$, and where j_l represents the spherical Bessel function of order l.

If M and M′ belong to the same n-mer, one finds:

$$\langle F(\mathbf{q}) F^*(\mathbf{q})\rangle_{\text{axis } i} = f_c^2 \left(60 + 2 \sum_{j>j'} \cos(q_{\parallel}(i) r_{jj'\parallel}(i)) J_0(q_{\perp}(i) r_{jj'\perp}(i)) \right)$$

where the indices j and j' refer to the atoms on a C_{60} molecule of the n-mer, with positions $\mathbf{r}_j$ and $\mathbf{r}_{j'}$ with respect to its center of mass, and where $r_{jj'\parallel}$(i) and $r_{jj'\perp}$(i) are the components of the vector $\mathbf{r}_{jj'} = \mathbf{r}_j - \mathbf{r}_{j'}$ along the axis i and perpendicular to it, respectively.

The diffuse scattering patterns simulated using the intensities calculated as above present an inherent noise or "speckle" effect due to the limited size of our model crystals. To remedy this artefact we have built a number of different model crystals with $4\times N_1\times N_2\times N_3$ molecules (the crystals differ because the dimers (or trimers) are selected at random) and the calculated intensities I_{D} have been averaged over these crystals. Typically, this averaging is efficient to smooth out the data and obtain satisfactory diffuse scattering patterns for 100 crystals, composed of $4 \times 10 \times 10 \times 10 = 4000$ C_{60} molecules.

References

1. V.D. Blank, S.G. Buga, G.A. Dubitsky, N.R. Serebryanaya, M. Yu. Popov, B. Sundqvist, Carbon **36**, 319 (1998)
2. B. Sundqvist, Adv. Phys. **48**, 1 (1999)
3. M.S. Dresselhaus, G. Dresselhaus, P.C. Eklund, *Science of fullerenes and carbon nanotubes* (Academic Press, San Diego, California, 1996)
4. G.A. Samara, L.V. Hansen, R.A. Assink, B. Morosin, J.E. Shirber, D. Loy, Phys. Rev. B **47**, 4756 (1993)
5. W.I.F. David, R.M. Ibberson, J. Phys: Condens. Matter **5**, 7923 (1993)
6. Y. Iwasa, T. Arima, R.M. Fleming, T. Siegrist, O. Zhou, R.C. Haddon, L.J. Rothberg, K.B. Lyons, H.L. Carter Jr., A.F. Hebard, R. Tycko, G. Dabbagh, J.J. Krajewski, G.A. Thomas, T. Yagi, Science, **264**, 1570 (1994)
7. J.-L. Hodeau, J.-M. Tonnerre, B. Bouchet-Fabre, M. Núñez-Regueiro, J.-J. Capponi, M. Perroux, Phys. Rev. B **50**, 10311 (1994)
8. V.D. Blank, V.N. Denisov, A.N. Ivlev, B.N. Mavrin, N.R. Serebryanaya, G.A. Dubitsky, S.N. Sulyanov, M. Yu. Popov, N.A. Lvova, S.G. Buga, G.N. Kremkova, Carbon **36**, 1263 (1998)
9. P.-A. Persson, U. Edlund, P. Jacobsson, D. Johnels, A. Soldatov, B. Sundqvist, Chem. Phys. Lett. **258**, 540 (1996)
10. V.A. Davydov, L.S. Kashevarova, A.V. Rakhmanina, V. Agafonov, R. Ceolin, H. Szwarc, Carbon **35**, 735 (1997)
11. A.M. Rao, Ping Zhou, Kai-An Wang, G.T. Hager, J.M. Holden, Ying Wang, W.-T. Lee, Xiang-Xin Bi, P.C. Eklund, D.S. Cornett, M.A. Duncan, I.J. Amster, Science **259**, 955 (1993)
12. G.W. Wang, K. Komatsu, Y. Murata, M. Shiro, Nature **387**, 583 (1997)
13. G. Oszlányi, G. Bortel, G. Faigel, L. Gránásy, G.M. Bendele, P.W. Stephens, L. Forró, Phys. Rev. B **54**, 11849 (1996)

14. T. Ozaki, Y. Iwasa, T. Mitani, Chem. Phys. Lett. **285**, 289 (1998)
15. A.V. Dzyabchenko, V. Agafonov, V.A. Davydov, J. Phys. Chem. **103**, 2812 (1999)
16. V.A. Davydov, L.S. Kashevarova, A.V. Rakhmanina, V. Agafonov, H. Allouchi, R. Ceolin, A.V. Dzyabchenko, V.M. Senyavin, H. Szwarc, T. Tanaka, K. Komatsu, J. Phys. Chem. B **103**, 1800 (1999)
17. D. Porezag, M.R. Pederson, T. Frauenheim, T. Köhler, Phys. Rev. B **52**, 14693 (1995)
18. V.A. Davydov, L.S. Kashevarova, A.V. Rakhmanina, V.M. Senyavin, R. Ceolin, H. Szwarc, H. Allouchi, V. Agafonov, Phys. Rev. B **61**, 11936 (2000)
19. V.A. Davydov, L.S. Kashevarova, A.V. Rakhmanina, V.M. Senyavin, O.P. Pronina, N.N. Oleinikov, V. Agafonov, R. Ceolin, H. Allouchi H. Szwarc, Chem. Phys. Lett. **333**, 224 (2001)
20. V.C. Long, J.L. Musfeldt, K. Kamarás, G.B. Adams, J.B. Page, Y. Iwasa, W.E. May, Phys. Rev. B **61**, 13191 (2000)
21. T. Wågberg, P.-A. Persson, B. Sundqvist, J. Phys. Chem. Solids **60**, 1989 (1999)
22. Y. Iwasa, K. Tanoue, T. Mitani, T. Yagi, Phys. Rev. B **58**, 16374 (1998)
23. P. Nagel, V. Pasler, S. Lebedkin, A. Soldatov, C. Meingast, B. Sundqvist, P.A. Persson, T. Tanaka, K. Komatsu, S. Buga, A. Inaba, Phys. Rev. B **60**, 16920 (1999)
24. V.A. Davydov, L.S. Kashevarova, A.V. Rakhmanina, V.M. Senyavin, O.P. Pronina, N.N. Oleinikov, V. Agafonov, R. Ceolin, H. Allouchi, H. Szwarc., JETP Lett. **68**, 928 (1998)
25. R. Moret, P. Launois, P.A. Persson, B. Sundqvist, Europhys. Lett. **40**, 55 (1997).
26. R. Moret, P. Launois, T. Wågberg, B. Sundqvist, Eur. Phys. J. B **15**, 253 (2000)
27. J. Winter, H. Kuzmany, A. Soldatov, P.-A. Persson, P. Jacobsson, B. Sundqvist, Phys. Rev. B **54**, 17486 (1996)
28. T. Wågberg, P. Jacobsson, B. Sundqvist, Phys. Rev. B **60**, 4535 (1999)
29. V. Agafonov, V.A. Davydov, L.S. Kashevarova, A.V. Rakhmanina, A. Kahn-Harari, P. Dubois, R. Céolin, H. Szwarc, Chem. Phys. Lett. **267**, 193 (1997)
30. M. Núñez-Regueiro, L. Marques, J.-L. Hodeau, O. Béthoux, M. Perroux, Phys. Rev. Lett. **74**, 278 (1995)
31. L. Marques, J.-L. Hodeau, M. Núñez-Regueiro, M. Perroux, Phys. Rev. B **54**, R12633 (1996)
32. P. Launois, S. Ravy, R. Moret, Int. J. Modern Phys. **13**, 253 (1999)
33. J.D. Axe, S.C. Moss, D.A. Neumann in *Solid State Physics: Advances in Research and Applications*, edited by H.E. Ehrenreich, F. Spaepen (Academic Press, New York, 1994), Vol. 48, pp. 149–224
34. J.R.D. Copley, K.H. Michel, J. Phys.: Condens. Matter **5**, 4353 (1993)
35. R. Moret, S. Ravy, J.-M. Godard, J. Phys. I France **2**, 1699 (1992)
36. P. Launois, S. Ravy, Roger Moret, Phys. Rev. B **52**, 5414 (1995)
37. J.M. Cabrera-Trujillo, J. Robles, Phys. Rev. B **64**, 165408 (2001)
38. P. Schiebel, K. Wulf, W. Prandl, G. Heger, R. Papoular, W. Paulus, Acta Cryst. A **52**, 176 (1996)
39. B. Narymbetov, V. Agafonov, V.A. Davydov, L.S. Kashevarova, A.V. Rakhmanina, A.V. Dzyabchenko, V.I. Kuvalov, R. Céolin, Chem. Phys. Lett. **367**, 157 (2003)
40. X. Chen, S. Yamanaka, Chem. Phys. Lett. **360**, 501 (2002)
41. R. Moret, P. Launois, T. Wågberg, B. Sundqvist, *Kirchberg Winterschool 2000: Electronic properties of novel materials/Molecular nanostructures,* AIP Conference Proc. **544**, 81 (2000)
42. S. Lebedkin, W.E. Hull, A. Soldatov, B. Renker, M.M. Kappes, J. Phys. Chem. B **104**, 4101 (2000)
43. A.V. Soldatov, G. Roth, A. Dzyabchenko, D. Johnels, S. Lebedkin, C. Meingast, B. Sundqvist, M. Haluska, H. Kuzmany, Science **293**, 680 (2001)